Journal of
Materials Chemistry A

Accepted Manuscript

This is an *Accepted Manuscript*, which has been through the RSC Publishing peer review process and has been accepted for publication.

Accepted Manuscripts are published online shortly after acceptance, which is prior to technical editing, formatting and proof reading. This free service from RSC Publishing allows authors to make their results available to the community, in citable form, before publication of the edited article. This *Accepted Manuscript* will be replaced by the edited and formatted *Advance Article* as soon as this is available.

To cite this manuscript please use its permanent Digital Object Identifier (DOI®), which is identical for all formats of publication.

More information about *Accepted Manuscripts* can be found in the **Information for Authors**.

Please note that technical editing may introduce minor changes to the text and/or graphics contained in the manuscript submitted by the author(s) which may alter content, and that the standard **Terms & Conditions** and the **ethical guidelines** that apply to the journal are still applicable. In no event shall the RSC be held responsible for any errors or omissions in these *Accepted Manuscript* manuscripts or any consequences arising from the use of any information contained in them.

Journal of Materials Chemistry A

Dynamic Article Links ►

Cite this: DOI: 10.1039/c0xx00000x

www.rsc.org/xxxxxx

Communication

NiAl layered double hydroxide@carbon nanopaticles hybrid electrode for high-performance asymmetric supercapacitors**

Xiaoxi Liu, Chong Wang, Yibo Dou, Awu Zhou, Ting Pan, Jingbin Han,* and Min Wei

Received (in XXX, XXX) Xth XXXXXXXXX 20XX, Accepted Xth XXXXXXXXX 20XX

DOI: 10.1039/b000000x

The NiAl layered double hydroxide (LDH)@carbon nanopaticles (CNPs) hybrid electrode was fabricated *via* a facile and cost-effective approach, which displays excellent pseudocapacitive behavior in asymmetric supercapacitors.

Nowadays, significant amount of efforts have been devoted to flexible, lightweight and environmentally friendly energy storage devices, as a result of the urgent need for sustainable and renewable power sources.[1, 2] Supercapacitors (SCs) represent a type of emerging energy storage devices that have attracted increasing attention due to their high power density, fast charging/discharging rate and excellent cycling stability.[3-6] Such outstanding properties make them promising in a wide range of applications from day-to-day electrical and portable electronics to industrial energy management, where high power density and long cycle-life are highly imperative. So far, pseudocapacitive transition-metal oxides/hydroxides have been extensively exploited in SCs with advantages of high capacitance, low cost and environment-friendliness.[7-9] However, the main obstacle is that they suffer from poor electrical conductivity and severe aggregation in particulate form, which consequently result in inferior high-rate performance and lower energy output.

To solve these problems, one effective approach is to anchor electroactive materials on specific substrate to fabricate ordered array electrode as well as to improve the conductivity via incorporation of highly conductive polymers or carbon materials (e.g., carbon nanotube, activated carbon and graphene). For instance, MnO_2/CNTs array, $Ni(OH)_2$/graphene nanoplate, V_2O_5/carbon nanotube and MnO_2/conductive polymer coaxial nanowire hybrid electrodes with improved electrochemical capacitive behavior have been explored.[1, 10-13] Even though these progresses in improving capacitance and durable stability, challenges for application of these materials in modern power sources still remain in a real supercapacitor manufacturing environment because of the high cost and complicated fabrication procedure. Therefore, it is of great significance to develop new hybrid electrodes as well as facile routes so as to obtain supercapacitors with high electrochemical performance.

Layered double hydroxides (LDHs), also known as anionic clays,[14, 15] have been intensively explored as pseudocapacitive materials due to their high redox activity, low cost and long cycle life.[16-20] Herein, we report the design and fabrication of NiAl-LDH nanoplatelet arrays (NPAs)@carbon nanoparticles (CNPs) hybrid electrodes on conductive fabrics (CFs) substrate for high-performance pseudocapacitor through a cost-effective process. LDH nanoplatelet arrays (NPAs) were firstly fabricated on the surface of conductive fabrics substrate *via* an *in situ* growth method, followed by incorporation of carbon nanoparticles (CNPs) on LDH nanoplatelets. The resulting NiAl-LDH@CNPs electrode displays rather high specific capacitance and rate capability, resulting from the enhanced electrochemically active surface area and electrical conductivity. In addition, a practical application of this new material has been demonstrated in an asymmetric all-solid-state SCs in which the LDH@CNPs serves as positive electrode and activated carbon (AC) as negative electrode.

The synthesis of LDH@CNPs hybrid electrode involves the growth of vertically aligned LDH NPAs *via* a hydrothermal reaction followed by CNPs coating through a vacuum filtration process, as illustrated in Fig. 1a. The well-interlaced conductive fabrics with a rather smooth surface and a diameter of ~9.5 μ m provide an electrically conductive network (Fig. 1b). By hydrothermal synthesis, large-scale of NiAl-LDH NPAs grew vertically on each fiber of the textile and have an uniform

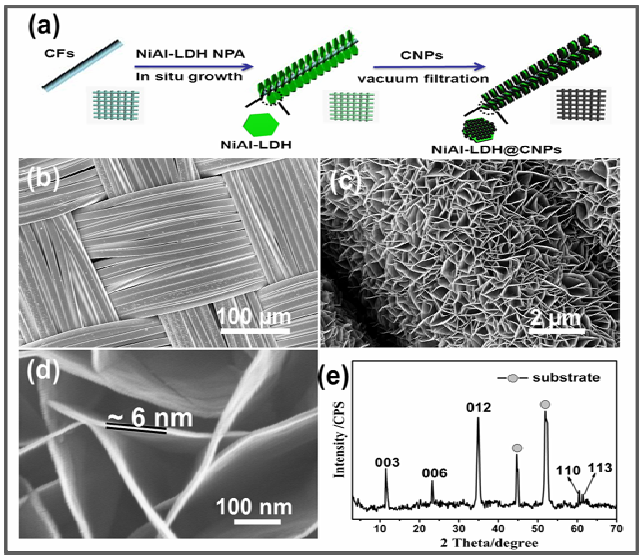

Fig. 1 (a) Schematic illustration for the fabrication of LDH@CNPs hybrid electrode; (b) SEM image of the conductive fibers (CFs); (c) and (d) top-view SEM images of the NiAl-LDH NPAs on the surface of CFs; (e) XRD pattern of as-prepared LDH NPAs on CFs.

structure (Fig. 1c, d). The obtained LDH NPAs present a porous network structure with a thickness of ~6 nm. The XRD pattern (Fig. 1e) shows a series of reflections at 11.7°, 23.5°, 34.8°, 59.7° and 60.9°, corresponding to the [003], [006], [012], [110] and [113] reflections of layered LDH phase. TEM image reveals a hexagonal morphology of a single LDH microcrystal, and the corresponding selected-area electron diffraction (SAED) pattern exhibits hexagonally arranged bright spots, indicating its single-crystal nature (ESI, Fig. S1).

An ideal supercapacitive material should have excellent electrical conductivity to support fast electron transport, especially at high charge-discharge rate. To enhance the conductivity of the as-grown LDH NPAs electrode, a thin layer of conductive CNPs was integrated to the surface of LDH nanoplatelets *via* vacuum filter to fabricate LDH@CNPs hybrid architecture. The CNPs (size: 12-18 nm) used in this study was obtained from candle soot by a low-cost and simple process (see details in the ESI, Fig. S2).

The well-defined and interconnected 3D network of the resulting architecture was revealed by typical SEM images (Fig. 2a–c). Numerous CNPs are densely coated on both sides of each LDH nanoplatelet, which maintain the original porous structure. The XPS spectrum of NiAl-LDH (Fig. 2d) shows two peaks located at 856.7 and 869.9 eV, respectively, corresponding to the 2p3/2 and 2p1/2 of Ni^{2+}. After the deposition of CNPs layer, both

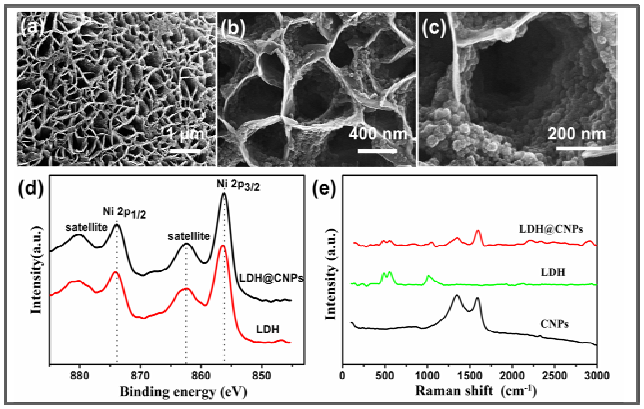

Fig. 2 (a-c) SEM images of LDH@CNPs hybrid material in different magnification; (d) Ni 2p XPS spectra of pristine LDH and LDH@CNPs; (e) Raman spectrum of the LDH, CNPs and LDH@CNPs samples.

the two peaks shift to lower energy levels (856.2 and 869.5 eV, respectively), as a result of the interaction between the LDH NPAs and CNPs. Moreover, the Raman spectrum (Fig. 3e) of the LDH@CNPs sample displays absorption peaks (478, 546 and 1054 cm^{-1}) originating from NiAl-LDH and two signals (1347 and 1603 cm^{-1}) attributed to CNPs, further verifying the formation of LDH@CNPs hybrid material.

In order to gain the optimized electrochemical performance of LDH@CNPs electrode, the cyclic voltammetry (CV) behaviour of the electrodes with various contents of CNPs were investigated in a three-electrode system (Fig. 3a). A pair of anodic/cathodic peaks are observed in all the CV curves as a result of the Faradic capacitive behavior, corresponding to the reversible redox of Ni^{2+}/Ni^{3+} associated with OH^-. The specific capacitance of bare LDH NPAs were calculated to be 627 F/g based on CV curve at a scan rate of 2 mV/s. After coating CNPs wrap, the specific capacitance of LDH@CNPs electrode (obtained from CV

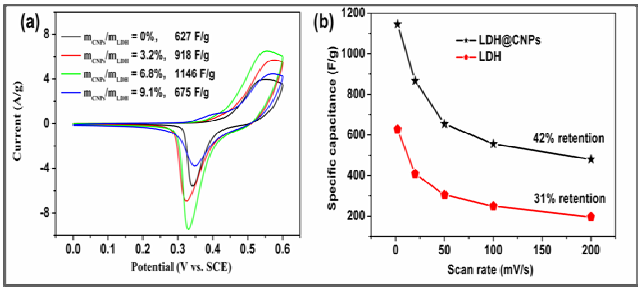

Fig. 3 (a) CV curves of LDH@CNPs hybrid electrodes with various m_{CNPs}/m_{LDH} ratios by using a three-electrode system in 1.0 M KOH solution; (b) the specific capacitance of LDH and LDH@CNPs electrodes at different scan rates.

measurement) increased at first to a maximum (1146 F/g) with the increase of CNPs:LDH weight ratio from 0 to 6.8% and then decreased upon further increasing CNPs loading. Moreover, the Galvanostatic charge–discharge curves (ESI, Fig. S3) is consistent with the results of CV analysis. Therefore, the LDH@CNPs with m_{CNPs}/m_{LDH}=6.8% was chosen as the optimum electrode for further evaluation of electrochemical performance. The overall mass loading of LDH@CNPs hybrid materials is 0.25 mg/cm^2. For the rate capability, the pristine LDH NPAs electrode shows a specific capacitance of 208 F/g at a scan rate of 200 mV/s, which remains only 31% of the initial capacitance at 2 mV/s. In comparison, the LDH@CNPs hybrid electrode exhibits a specific capacitance of 478 F/g at 200 mV/s, with a retention of 42% (Fig. 3b), demonstrating its superior high-rate capability. In addition, the electrochemical impedance spectroscopy (EIS) was applied to study the ion diffusion and electron transfer properties of the obtained hybrid electrode (Fig. S4). The equivalent series resistance (ESR) was only 1.4 Ω for the sample of LDH@CNPs (area: $1cm^2$), much lower than that of pure LDH NPAs (3.62 Ω; $1cm^2$), indicating the better electrical conductivity of LDH@CNPs electrode. The enhanced capacitance and high-rate capability of the LDH@CNPs electrode are attributed to the improvement in electrical conductivity of the electrode after coating with CNPs.

To demonstrate the prospect of LDH@CNPs electrode for parctical application, a sandwich-shaped asymmetric all-solid-state supercapacitor was assembled by using the LDH@CNPs and active carbon (AC) as positive and negative electrode, respectively (Fig. 4a, see details in the ESI, Fig. S5). Fig. 4b shows the CV curves of LDH@CNPs//AC all-solid-state supercapacitor at different scan rates with a voltage window of 0-1.6V, which display a quasi-rectangular geometry feature without apparent redox peaks. This is related to the high conductivity of LDH@CNPs hybrid electrode and fast redox reaction with PVA/KOH solid electrolyte. Galvano-static charge-discharge curves with different current densities (Fig. 4c) also exhibit a typical pseudocapacitive behavior, with coulombic efficiency of ~93%. The specific capacitances of the LDH@CNPs//AC and LDH//AC supercapasitors as a function of current density were further investigated (Fig. 4d). The LDH//AC capacitor shows a specific capacitance of 105 F/g at 1 A/g and 35 F/g at 10A/g, respectively, with a loss of ~67% of initial capacitance. In contrast, the LDH@CNPs//AC capacitor exhibits a specific capacitance of 138 F/g at 1 A/g, and 79 F/g at 10 A/g with a retention of 57.2%. The better rate performance highlights the

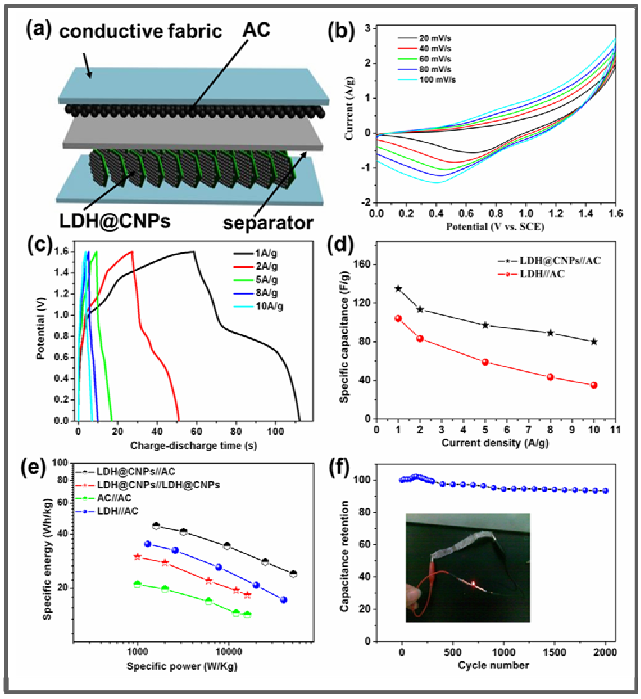

Fig. 4 (a) Schematic illustration of the LDH@CNPs//AC asymmetric SC; (b) CV curves of the LDH@CNPs//AC supercapacitor at different scan rates; (c) charge–discharge curves of the LDH@CNPs//AC at different current densities; (d) specific capacitance of LDH//AC and LDH@CNPs//AC asymmetric SC at different current densities; (e) Ragone plots of LDH@CNPs//AC, LDH//AC, AC//AC and LDH@CNPs//LDH@CNPs supercapacitors; (f) cycling stability of the LDH@CNPs//AC during charge–discharge test at 10 A/g (inset: a digital picture shows two highly flexible devices in series are lighting a red light-emitting-diode).

advantage of electrical conductivity of the electrode after coating CNPs, which would definitely facilitate the electron transport. Fig. 4e shows the specific energy *vs.* specific power plot of the four SCs (LDH@CNPs//AC, LDH//AC, AC//AC, LDH@CNPs//LDH@CNPs) as the charge-discharge current increased from 1 to 10 A/g. The specific energy values for LDH@CNPs//LDH@CNPs, AC//AC, LDH//AC are 35.3, 21.0 and 30.2 Wh/kg at 1 A/g. In contrast, the LDH@CNPs//AC supercapacitor displays largely enhanced specific energy: the highest specific energy of 47.7 Wh/kg (1 A/g) and the maximum specific power of 51 kW/kg (10 A/g) were achieved. Furthermore, the energy density of LDH@CNPs//AC supercapacitor is even superior to graphene hydrogel//MnO_2 (23.2 Wh/kg)[21], MnO_2 nanowire@graphene composite//graphene (30.4 Wh/kg)[22], and NiO//reduced graphene oxide (39.9 Wh/kg)[23] asymmetric SCs.

Cycling capability is one key requirement in practical applications. The cycling life test on the LDH@CNPs//AC supercapacitor was carried out at a current density of 10 A/g using galvanostatic charge-discharge technique, and the result shows a capacitance retention of 88.9% over 2000 cycles (Fig.4f). To further demonstrate the application prospect of the asymmtric supercapacitor, two single units were connected in series to light a red light-emitting-diode (Fig. 4f), which exhibits an enhanced potential window up to 2.8 V (Fig. S6). In addition, the change in CV curves collected with different bending angles is subtle and acceptable (Fig. S7), and the LDH@CNPs//AC supercapacitor displays rather low leakage current and good self-discharge performance (see details in the ESI, Fig. S8), demonstrating its capability as a flexible energy storage device for practical applications.

In conclusion, a facile and cost-effective approach was developed to fabricate high-performance asymmtric supercapacitor based on LDH@CNPs//AC hybrid structure. The resulting supercapacitor exhibits excellent capacitive performance, including high specific capacitance, good cycling capability and high energy density. The improved capacitance and rate capability are attributed to the enhanced electrical conductivity via the incorporation of CNPs, in combination with facile ion diffusion path provided by the 3D macroporous sructure. Therefore, this asymmtric supercapacitor offers great promise for application in flexible and lightweight energy storage devices.

This work was supported by the 863 Program (Grant No. 2013AA032501), the National Natural Science Foundation of China, the Scientific Fund from Beijing Municipal Commission of Education (20111001002), the Fundamental Research Funds for the Central Universities and the Doctoral Fund of Ministry of Education of China (20120010120010).

Notes and References

State Key Laboratory of Chemical Resource Engineering, Beijing University of Chemical Technology, Beijing 100029, P. R. China, Fax: 86-10-64425385;Tel:86-10-64412131; Email: hanjb@mail.buct.edu.cn

1. R. Liu and S. B. Lee, *J. Am. Chem. Soc.*, 2008, **130**, 2942.
2. Y. Li, K. Sheng, W. Yuan and G. Shi, *Chem. Commun.*, 2013, **49**, 291.
3. P. J. Hall, M. Mirzaeian, S. I. Fletcher, F. B. Sillars, A. J. R. Rennie, G. O. Shitta-Bey, G. Wilson, A. Cruden and R. Carter, *Energy Environ. Sci.*, 2010, **3**, 1238.
4. P. Simon and Y. Gogotsi, *Nat. Mater.*, 2008, **7**, 845.
5. P. Yang, X. Xiao, Y. Li, Y. Ding, P. Qiang, X. Tan, W. Mai, Z. Lin, W. Wu, T. Li, H. Jin, P. Liu, J. Zhou, C. P. Wong and Z. L. Wang, *ACS Nano*, 2013, **7**, 2617.
6. S. M. Paek, J. H. Kang, H. Jung, S. J. Hwang and J. H. Choy, *Chem. Commun.*, 2009, **48**, 7536.
7. J. Liu, J. Jiang, C. Cheng, H. Li, J. Zhang, H. Gong and H. J. Fan, *Adv. Mater.*, 2011, **23**, 2076.
8. G. Zhao, J. Li, L. Jiang, H. Dong, X. Wang and W. Hu, *Chem. Sci.*, 2012, **3**, 433.
9. L. Yuan, X.-H. Lu, X. Xiao, T. Zhai, J. Dai, F. Zhang, B. Hu, X. Wang, L. Gong, J. Chen, C. Hu, Y. Tong, J. Zhou and Z. L. Wang, *ACS Nano*, 2012, **6**, 656.
10. M. Sathiya, A. S. Prakash, K. Ramesha, J. M. Tarascon and A. K. Shukla, *J. Am. Chem. Soc.*, 2011, **133**, 16291.
11. S. Yang, X. Wu, C. Chen, H. Dong, W. Hu and X. Wang, *Chem. Commun.*, 2012, **48**, 2773.
12. Y. Yang, D. Kim, M. Yang and P. Schmuki, *Chem. Commun.*, 2011, **47**, 7746.
13. J. Yan, Z. Fan, W. Sun, G. Ning, T. Wei, Q. Zhang, R. Zhang, L. Zhi and F. Wei, *Adv. Funct. Mater.*, 2012, **22**, 2632.
14. M.-Q. Zhao, Q. Zhang, W. Zhang, J.-Q. Huang, Y. Zhang, D. S. Su, and F. Wei, *J. Am. Chem. Soc.*, 2010, **132**,14739.
15. Q. Wang and D. O'Hare, *Chem. Rev.*, 2012, **112**, 4124.
16. L. Zhang, X. Zhang, L. Shen, B. Gao, L. Hao, X. Lu, F. Zhang, B. Ding and C. Yuan, *J. Power Sources*, 2012, **199**, 395.
17. L. Su, X. Zhang, C. Yuan and B. Gao, *J. Electrochem. Soc.*, 2008, **155**, A110.
18. J. Zhao, Z. Lu, M. Shao, D. Yan, M. Wei, D. G. Evans and X. Duan, *RSC Adv.*, 2013, **3**, 1045.
19. X. Guo, F. Zhang, D. G. Evans and X. Duan, *Chem. Commun.*, 2010, **46**, 5197.
20. Z. Lu, W. Zhu, X. Lei, G. R. Williams, D. O'Hare, Z. Chang, X. Sun and X. Duan, *Nanoscale*, 2012, **4**, 3640.

21. H. Gao, F. Xiao, C. B. Ching and H. Duan, *ACS Appl. Mater. Interfaces*, 2012, **4**, 2801.
22. Z.-S. Wu, W. Ren, D.-W. Wang, F. Li, B. Liu and H.-M. Cheng, *ACS Nano*, 2010, **4**, 5835.
23. F. Luan, G. Wang, Y. Ling, X. Lu, H. Wang, Y. Tong, X. X. Liu and Y. Li, *Nanoscale*, 2013, **5**, 7984.